Influence of Maltodextrin on the Physicochemical Properties of Chitosan- and Starch-Based Biopolymeric Matrices for Active Packaging

Mariangel Caro-Reyes [†], Carolina Arias-Gutiérrez [†], María Esther Treviño-Martínez, Aldo Rafael Vazquez-Arce, José Alfredo Beristain-Bautista, Carolina Caicedo [*], Abril Fonseca-García [*]

Posted Date: 8 May 2026

doi: 10.20944/preprints202605.0565.v1

Keywords: chitosan; controlled-release systems; maltodextrin; polymeric matrix; starch

 doi:10.20944/preprints202605.0565.v1

Article

Influence of Maltodextrin on the Physicochemical Properties of Chitosan- and Starch-Based Biopolymeric Matrices for Active Packaging

Mariangel Caro-Reyes [1,†], Carolina Arias-Gutiérrez [1,†], María Esther Treviño-Martínez [2], Aldo Rafael Vazquez-Arce [3], José Alfredo Beristain-Bautista [4], Carolina Caicedo [1,*] and Abril Fonseca-García [5,*]

[1] Energías Research Group, Faculty of Engineering, Unidad Central del Valle del Cauca (UCEVA), Carrera 17a 48-144, Tuluá 763022, Colombia

[2] Centro de Investigación en Química Aplicada (CIQA), Blvd. Enrique Reyna Hermosillo 140, Saltillo 25294, Coahuila, México

[3] Centro de Biotecnología Industrial, Servicio Nacional de Aprendizaje (SENA), Colombia

[4] Ingeniería en Nanotecnología, Tecnológico Nacional de México / Instituto Tecnológico Superior de Poza Rica, Luis Donaldo Colosio Murrieta S/N, Poza Rica de Hidalgo, México

[5] CIQA-Secretaría de Ciencia, Humanidades, Tecnología e Innovación (SECIHTI), Enrique Reyna Hermosillo Boulevard 140, Saltillo, Coahuila de Zaragoza 25253, México

* Correspondence: ccaicedoc@uceva.edu.co (C.C.); abril.fonseca@ciqa.edu.mx (A.F.-G.)

† These authors contributed equally to this work.

Abstract

In this study, the effect of incorporating maltodextrin into films composed of thermoplastic starch and chitosan was evaluated with the aim of improving their physicomechanical properties. X-ray diffraction revealed greater organization in sample TPS-CH-M3 compared with TPS-CH-M0 and TPS-CH-M5, indicating a balanced semicrystalline structure. Thermal analyses showed an increase in the glass transition temperature from 63.0 °C to 72.6 °C and a shift of the main degradation step from 308 °C to 311 °C, reflecting enhanced thermal stability. The contact angle decreased from 89.5° to 74.0°, confirming increased hydrophilicity. SEM micrographs revealed a homogeneous surface in TPS-CH-M0 and controlled roughness in TPS-CH-M3. Mechanical tests recorded the highest tensile strength (12.5 MPa) and elongation at break (18%) for TPS-CH-M3. FTIR spectra showed physical interactions without new chemical bands, and colorimetric analysis indicated an increase in yellow tonality, which is suitable for packaging and coatings of light-sensitive foods.

Keywords: chitosan; controlled-release systems; maltodextrin; polymeric matrix; starch

1. Introduction

The development of polymeric biomaterials and composite materials has enabled more precise administration of active ingredients, thereby contributing to enhanced therapeutic efficacy across a wide range of treatments. These systems have supported advances in drug delivery [1], tissue engineering, and regenerative medicine [2], by improving release control and functional compatibility with the biological environment factors that directly influence host responses [3]. Within these applications, polymeric matrices have emerged as a promising alternative due to their capacity to encapsulate and release active ingredients in a controlled manner [4,5]. Their use spans several administration routes, including oral [6], transdermal [7], and parenteral delivery [8], as well as the development of functional biomaterials for tissue engineering [2]. Research on these matrices remains essential for improving the bioavailability of active ingredients, reducing dosing frequency, minimizing adverse effects, and enhancing dosing precision [9].

 doi:10.20944/preprints202605.0565.v1

Over the past two decades, polymeric hydrogels have been extensively studied for their capacity to form hydrated three-dimensional networks that enable the sustained release of bioactive compounds [10,11]. Among the most widely employed materials are gelatin, due to its biocompatibility and its ability to form thermoreversible hydrogels [12,13] and chitosan, which supports the development of pH- and temperature-responsive systems owing to its cationic nature and mucoadhesive properties [14,15]. Maltodextrin is also frequently incorporated because of its amorphous structure and the presence of hydroxyl groups. This compound has been used as a matrix for the encapsulation of hydrophilic drugs such as ascorbic acid [16], caffeine [17], and acetaminophen [18], as well as hydrophobic compounds including curcumin [19], resveratrol [20], and ferulic acid [21], commonly in combination with starch, lipids, or other biopolymers [22,23]. Its ability to form hydratable networks and modulate matrix structure enhances both stability and release efficiency [24]. Recent studies have demonstrated that maltodextrin can be transformed into hydrogel-like structures via sustainable transesterification processes, with promising applications in drug delivery [25]. Owing to its performance as a versatile and functional excipient, it is considered a second-generation polymeric carrier, representing an intermediate category between conventional excipients and advanced delivery systems [25].

In the design of polymeric matrices, surface energy plays a critical role in determining miscibility, structural cohesion, and system stability [26]. To enhance compatibility between materials such as thermoplastic starch and chitosan, plasticizers such as glycerol are commonly incorporated to increase chain mobility, reduce surface energy, and promote the formation of flexible matrices [27–29]. However, in the absence of a structural co-formulant, the blend may remain heterogeneous. In this context, maltodextrin due to its low surface energy and high solubility facilitates dispersion between phases and improves the thermal and mechanical stability of the system [30,31]. Nonetheless, developments in the design of polymeric matrices remain limited with respect to their application in the delivery of active ingredients, particularly regarding mechanical stability, release control, and compatibility with diverse compounds [31,32].

During this study, different samples of polymeric matrices were formulated with varying concentrations of maltodextrin. These samples were subjected to mechanical testing to evaluate their strength and structural stability. In addition, their physicochemical properties were analyzed to determine their suitability for the delivery of active pharmaceutical ingredients (APIs). It is expected that the results of this research will have a significant impact on the biomedical industry by enabling the development of more efficient and versatile delivery vehicles, since the use of maltodextrin can improve the bioavailability of pharmaceutical compounds, facilitating more precise dosing and reducing adverse effects associated with other delivery systems [18,22]. This study aims to determine the influence of maltodextrin concentration on the formation of matrices suitable for the encapsulation and/or delivery of APIs, evaluating the mechanical and functional properties required for this type of application. Optimizing these parameters will allow the design of more efficient and versatile delivery vehicles in the biomedical field.

2. Materials and Methods

2.1. Materials

Native cassava starch (TPS), with an amylose content of 18.1% and an amylopectin content of 81.9%, was supplied by Industrias Ragar S.A. de C.V. Low-molecular-weight chitosan (CH), with a degree of deacetylation greater than 75%, was obtained from Sigma-Aldrich. Pharmaceutical-grade maltodextrin (M) was purchased from ADISA. Reactive-grade glycerol was acquired from Meyer de México, and glacial acetic acid from Merck.

 doi:10.20944/preprints202605.0565.v1

2.2. Preparation of Films

Film-forming solutions were prepared from TPS–CH–M polymer blends in a 60:20:20 ratio, respectively. The TPS solution was prepared at 5% w/w in distilled water, incorporating glycerol at 25% relative to the total polymer mass in the film-forming solution. The CH solution was prepared at 2% w/w, using a 1% w/w acetic acid solution as the solvent. The M solution was prepared in distilled water at concentrations of 0, 1, 3, and 5% w/w. Consequently, four formulations were obtained: M 0%, M 1%, M 3%, and M 5%. The polymer blend was homogenized under magnetic stirring and heated at 70 °C for 10 min, a temperature at which starch gelatinization occurs, thereby yielding the film-forming solutions. Table 1 lists the precursor contents used for the preparation of these solutions.

Table 1. Formulation of the prepared films.

Reagent	Formulation (g) for 100 g of film-forming solution			
	Malto 0%	**Malto 1%**	**Malto 3%**	**Malto 5%**
Starch	3.0	3.0	3.0	3.0
Chitosan	0.4	0.4	0.4	0.4
Maltodextrin	0.0	0.2	0.6	1.0
Glycerol	0.85	0.9	1.0	1.1
Acetic acid	0.2	0.2	0.2	0.2

Following homogenization, the film-forming solutions were degassed under vacuum to remove residual air bubbles generated during stirring after starch gelatinization. The bubble-free solutions were then poured into a rectangular acrylic mould and dried in a convection oven at 60 °C for 3 h to obtain the final films.

2.3. Physicochemical Characterization

2.3.1. Crystalline Structure (XRD)

X-ray diffraction patterns of the samples were obtained using a Bruker D8 Advance powder diffractometer equipped with monochromatic Cu Kα radiation (λ = 1.5418 Å) in Bragg–Brentano configuration, over an angular range of 4–50° (2θ).

2.3.2. Thermal Analysis

Thermogravimetric analysis (TGA) was conducted using a TGA Q500 analyzer (TA Instruments). Samples were placed in aluminium crucibles and heated from room temperature to 800 °C at a rate of 10 °C/min under a nitrogen atmosphere with a flow rate of 60 mL/min.

2.3.3. Wettability

Wettability was assessed by measuring the contact angle formed by a sessile drop of distilled water on the surface of the films. A Rame-Hart Instrument Co. video goniometer was used for all measurements. A 4 µL droplet of deionized water was deposited on the side of the film that did not contact the mould during formation, using a micropipette to ensure precise droplet volume. Six measurements were performed on the dry surface of each sample. Images were captured and contact angles were calculated using ImageJ software.

 doi:10.20944/preprints202605.0565.v1

2.3.4. Morphological Analysis by Scanning Electron Microscopy (SEM)

Film morphology was examined using a NeoScope JCM-6000 scanning electron microscope (JEOL) operated at 10 kV under high vacuum. Prior to imaging, the films were coated with a conductive gold–palladium layer using a DESK II sputtering system (Denton Vacuum Inc.).

2.3.5. Mechanical Properties

Before mechanical testing, the films were conditioned in a controlled-environment chamber at 50 ± 5% relative humidity and 23 ± 2 °C. Mechanical properties were evaluated using a universal testing machine (electromechanical series SFM-100KN, United Testing Systems Canada Limited). Tensile tests were performed at a crosshead speed of 50 mm/min with an initial grip separation of 25 mm, following ASTM D882-18. All tests were conducted in triplicate.

2.3.6. Fourier Transform Infrared Spectroscopy (FTIR)

The vibrational modes of the functional groups present in the samples were analyzed using Fourier transform infrared spectroscopy (FTIR) with a Nicolet iS10 spectrophotometer (Thermo Fisher Scientific). Measurements were performed by attenuated total reflectance (ATR) over a spectral range of 4000 cm^{-1} – 650 cm^{-1}.

2.3.7. Colorimetry

Colour parameters were determined using a portable spectrophotometer (MiniScan EZ 4500L, HunterLab, Reston, VA, USA) following the CIELab scale, which provides the coordinates L*, a*, and b* (Gómez-Aldapa et al., 2021). The films were placed on white copy paper used as the standard, with colour coordinate values of L* = 91.76, a* = 2.14, and b* = −10.64.

2.3.8. Statistical Analysis

Means and standard deviations are reported. Analysis of variance (ANOVA) was employed to compare differences in the mean values of the film characteristics. Post hoc comparisons were conducted using Tukey's test with a significance level of 0.05. All statistical analyses were performed using IBM® SPSS® Statistics 25.

3. Results and Discussion

3.1. X-Ray Diffraction (XRD) Analysis

The diffractograms presented in Figure 1 show characteristic peaks in the low-angle region (~9–10°) and main reflections at approximately 20.1°, 21.8°, 19.6°, and 21.5° for samples TPS-CH-M0, TPS-CH-M1, TPS-CH-M3, and TPS-CH-M5, respectively. These patterns indicate the coexistence of amorphous and semicrystalline phases. In sample TPS-CH-M0, a broad band between 15.0° and 25.0°, with a maximum at 20.1°, is observed, suggesting a predominantly amorphous matrix resulting from a low degree of internal molecular organization [33,34].

The incorporation of increasing concentrations of maltodextrin in the TPS-CH matrix induces structural rearrangements within the system, as evidenced by shifts in peak position and changes in peak intensity [35]. Table 2 summarizes the calculated area under the curve for all observed peaks. Sample TPS-CH-M3 exhibited the highest total peak area (24,619.4), indicating a more efficient distribution of ordered domains within the matrix [27]. In contrast, TPS-CH-M5 showed a reduced total area (18,941.4), suggesting a more localized ordering that does not translate into a globally enhanced crystalline structure. The TPS-CH-M1 formulation displayed intermediate behaviour, with a lower peak area (11,846.0), corresponding to a reduced degree of structural ordering. Overall, these findings indicate that a maltodextrin concentration of 3% represents an optimal condition for

 doi:10.20944/preprints202605.0565.v1

promoting the formation of semicrystalline domains without compromising the homogeneity of the system.

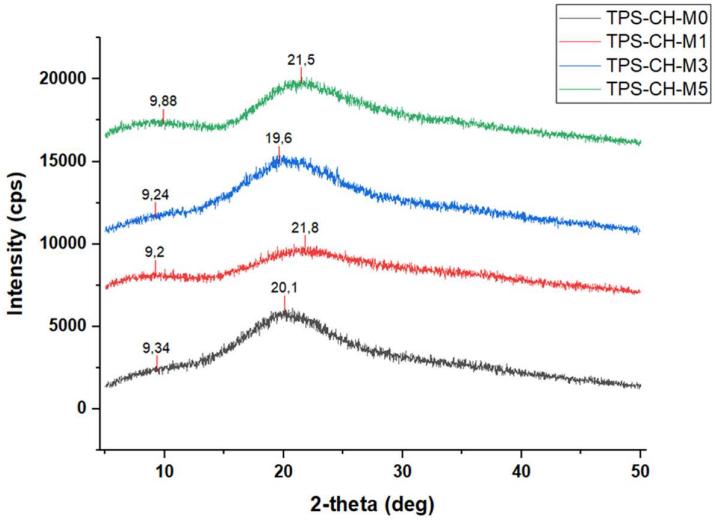

Figure 1. X-ray diffraction (XRD) patterns of TPS-CH-M0, TPS-CH-M1, TPS-CH-M3, and TPS-CH-M5.

Table 2. Area under the curve and peak intensity of characteristic reflections for each blend.

Sample	2θ (peak 1)	Intensity (peak 1)	Area 1	2θ (peak 2)	Intensity (peak 2)	Area
TPS-CH-M0	9.3	2741.6	1270.7	20.1	6400.0	23316.7
TPS-CH-M1	9.2	853.6	1785.4	21.8	10028.3	11846.0
TPS-CH-M3	9.2	12040.0	866.3	19.6	15390.0	24619.4
TPS-CH-M5	9.2	17701.6	2045.4	21.5	20218.3	1841.4

3.2. Simultaneous Thermal Analysis (TGA–DSC)

Figure 2 shows that the glass transition temperature (T_g) increases progressively with rising maltodextrin concentration. As reported in Table 3, sample TPS-CH-M0 exhibits a T_g of 63.0 °C, while TPS-CH-M1 reaches 70.4 °C, TPS-CH-M3 71.5 °C, and TPS-CH-M5 72.6 °C. This continuous increase suggests that the addition of maltodextrin restricts molecular mobility within the material, thereby enhancing its structural rigidity [36]. Such behaviour is typical of polymeric systems in which an additive strengthens interchain cohesion, limits segmental motion, and consequently raises T_g (dos Santos, De Sousa, and Gregorio, 2013) [37]. In contrast, the melting temperature (T_m) exhibits a non-linear trend. TPS-CH-M0 shows a T_m of 121.1 °C, which decreases to 100.2 °C for TPS-CH-M1, increases to 113.2 °C for TPS-CH-M3, and decreases again to 108.2 °C for TPS-CH-M5. This variability suggests that maltodextrin influences the crystalline organization of the material. When an additive disrupts molecular packing, less ordered regions can form, reducing thermal stability and consequently lowering the melting temperature [30]. Previous research has demonstrated that reduced crystallinity in polymeric systems leads to lower T_m values, as materials with fewer well-defined crystalline domains melt at lower temperatures [38].

Analysis of the heat flow and the area under the curve corroborates these observations. In the glass transition region, the area increases with higher maltodextrin concentrations, indicating that greater energy is required for the material to overcome T_g. This supports the interpretation that molecular interactions become stronger as maltodextrin content increases, hindering the transition from the glassy to the rubbery state [39]. However, the melting enthalpy does not follow a uniform trend, suggesting that crystallinity is not affected homogeneously, likely due to irregular interactions

 doi:10.20944/preprints202605.0565.v1

between maltodextrin and the polymer matrix [30]. Overall, these results align with previous studies on the thermal modification of polymers through additive incorporation, in which reinforcements or fillers typically increase T_g, while variations in Tm depend on the degree of compatibility between the amorphous and crystalline phases [37]. In systems where the additive interferes with crystallization, less organized domains may form, resulting in reduced thermal stability [36,39].

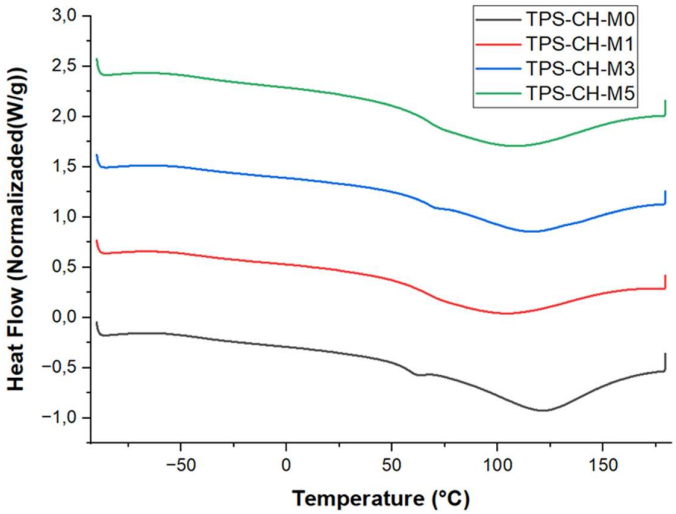

Figure 2. DSC curves of TPS-CH-M0, TPS-CH-M1, TPS-CH-M3, and TPS-CH-M5 in the temperature range from −90 °C to 180 °C.

Table 3. Area under the curve and heat flow in the different thermal transitions of the material.

Sample	T_g	Heat Flow	Area	T_m	Heat Flow	Area
TPS-CH-M0	63.0	-0.5	12.7	121.1	-0.9	31.0
TPS-CH-M1	70.4	-0.6	11.9	100.2	-0.7	24.1
TPS-CH-M3	71.5	-0.5	10.2	113.2	-0.8	25.8
TPS-CH-M5	72.6	-0.7	16.1	108.2	-0.9	30.0

In Figure 3, all formulations exhibit a similar degradation profile characterized by three main weight-loss stages, consistent with reports for starch- and chitosan-based polymeric systems [36,38]. The first weight-loss event, occurring between 100 °C and 120 °C, corresponds to the evaporation of adsorbed water and the desorption of residual moisture, as expected in hydrophilic biopolymers such as starch, chitosan, and maltodextrin [30]. At this stage, films containing maltodextrin (TPS-CH-M1, TPS-CH-M3, and TPS-CH-M5) show more pronounced mass loss than TPS-CH-M0, confirming the high water affinity of maltodextrin due to its hydroxyl groups, which readily form hydrogen bonds [40]. This behaviour aligns with observations in polysaccharide films where maltodextrin incorporation enhances moisture absorption and retention [41].

The second stage, corresponding to the major degradation of the polymer matrix, occurs between 300 and 320 °C, with degradation peaks between 308 and 311 °C for all formulations. In this region, cleavage of glycosidic bonds and decomposition of the polysaccharide chains take place [36]. Weight loss in this stage ranges from approximately 67% to 70%, indicating that this is the most intense degradation phase of the matrix [30]. Notably, TPS-CH-M3 exhibits distinct behaviour: its maximum degradation peak shifts to 311 °C, and the mass loss proceeds less abruptly than in TPS-CH-M0, TPS-CH-M1, and TPS-CH-M5. This suggests a more gradual and stable decomposition process [27]. These results indicate that a 3% maltodextrin content enhances intermolecular

 doi:10.20944/preprints202605.0565.v1

interactions, strengthening internal matrix cohesion, consistent with previous reports on polymer compatibilization [26]. This finding also agrees with the XRD analysis, which showed that TPS-CH-M3 exhibited a higher degree of structural order [42].

In the third stage, occurring between 600 and 640 °C, a secondary degradation event associated with carbonization and the formation of carbonaceous residues is observed. Final residue values range from 20% to 22%, with TPS-CH-M5 presenting the highest residue (21.65%), which may be attributed to heterogeneous microdomains that are less volatile and more resistant to complete decomposition [39]. This behaviour is consistent with previous studies showing that the incorporation of polysaccharides or plasticizers can promote the formation of more thermally stable carbonaceous residues [21].

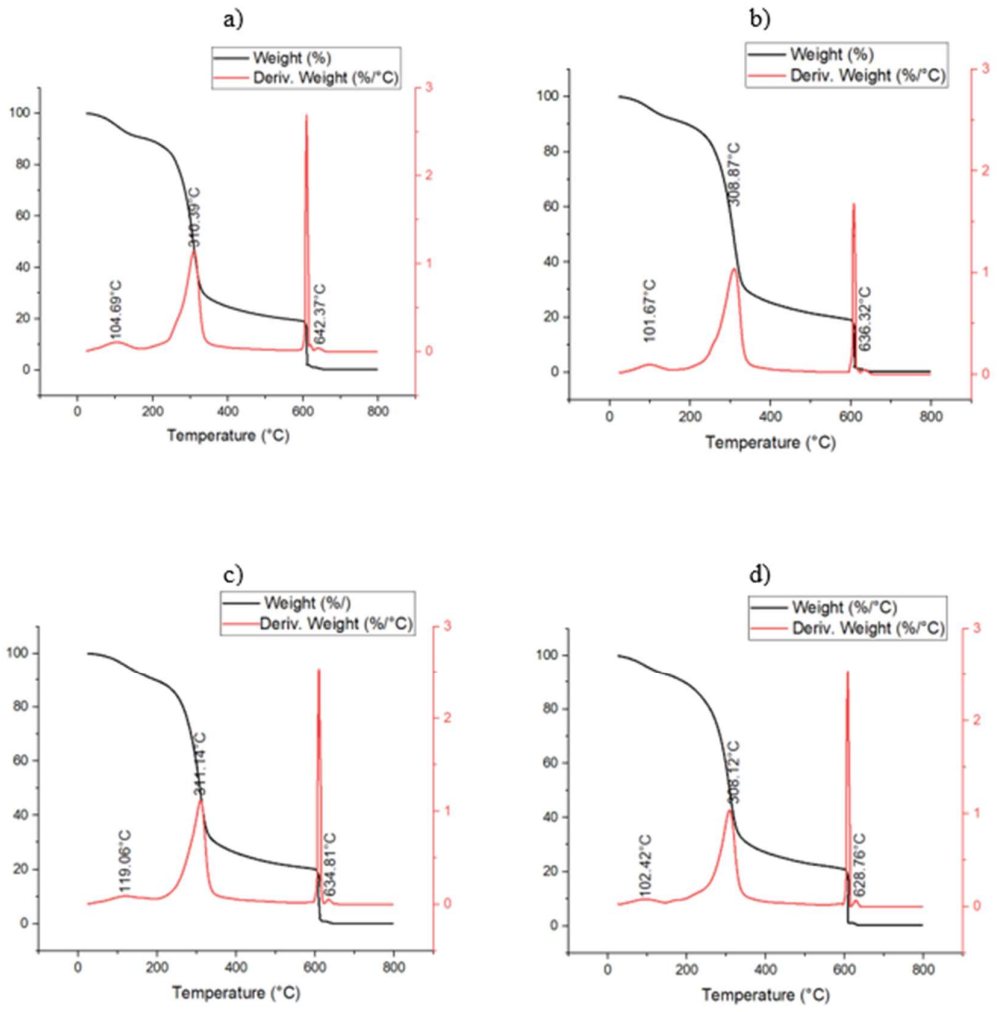

Figure 3. TGA curves of (a) TPS-CH-M0, (b) TPS-CH-M1, (c) TPS-CH-M3, and (d) TPS-CH-M5.

3.3. Contact Angle

The contact angle data are presented in Table 4, which shows a decreasing trend as the maltodextrin content in the films increases. Sample TPS-CH-M0 exhibits the highest contact angle (89.5° ± 0.57), indicating a lower affinity for water. As the maltodextrin concentration increases, the contact angle progressively decreases; this reduction reflects higher water affinity and, consequently, greater wettability [40].

 doi:10.20944/preprints202605.0565.v1

This behaviour can be attributed to the chemical structure of maltodextrin, a polysaccharide composed of glucose chains with numerous hydroxyl (–OH) groups that are highly polar and capable of forming hydrogen bonds with water. These interactions enhance the hydrophilicity of the film surface [43]. Similarly, the addition of hydrophilic plasticizers or sugars to protein- or polysaccharide-based matrices has been reported to increase water affinity by reducing internal cohesion between polymer chains and facilitating water diffusion into the matrix [41].

Table 4. Contact angle (°) and representative images for films with different maltodextrin concentrations.

Sample	Contact angle (°)	Picture
TPS-CH-M0	89.5 ± 0.57	
TPS-CH-M1	86.0 ± 2.44	
TPS-CH-M3	77.0 ± 1.82	
TPS-CH-M5	74.0 ± 2.94	

3.4. Scanning Electron Microscopy (SEM)

The morphological profiles of films without maltodextrin and with different maltodextrin concentrations were analyzed by scanning electron microscopy (SEM), as shown in Figure 4. The control sample (TPS-CH-M0) exhibits a relatively smooth and homogeneous surface; however, even in this formulation, the presence of fissures or cracks is evident, and these become more pronounced as the maltodextrin content increases. In the formulations containing maltodextrin (TPS-CH-M1, TPS-CH-M3, and TPS-CH-M5), increased surface roughness is observed, accompanied by striations, microdomains, and a more prominent cracking pattern. This behaviour may be associated with the internal redistribution of polymeric phases and with stresses generated during water evaporation in the drying stage, which are exacerbated by the hydrophilic nature of maltodextrin. At higher concentrations, as in TPS-CH-M5, the surface adopts a wrinkled and fragmented appearance, consistent with reported observations of increased surface irregularity and wrinkled structures upon incorporation of high maltodextrin contents [27]. No visible porosity was detected in any formulation, indicating that, despite the morphological changes, the films retained their superficial structural integrity.

 doi:10.20944/preprints202605.0565.v1

Table 5. SEM micrographs of TPS-CH-M films at magnifications of 1000×, 500×, and 100×.

Sample	1000×	500×	100×
TPS-CH-M0	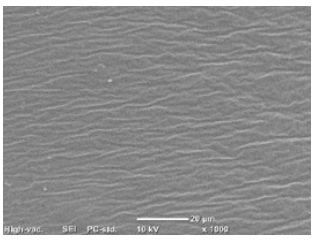	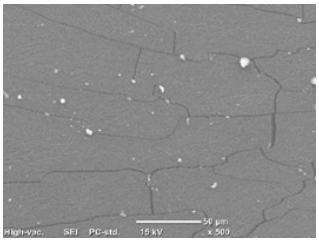	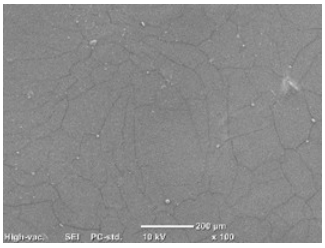
TPS-CH-M1	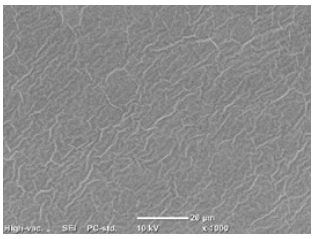	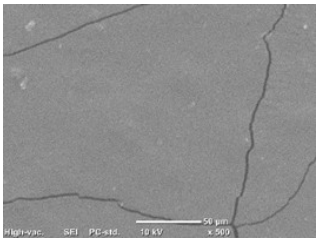	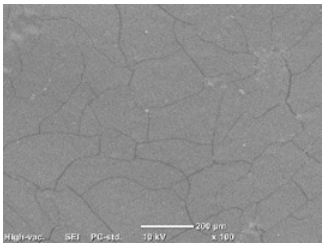
TPS-CH-M3	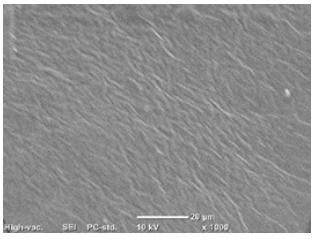	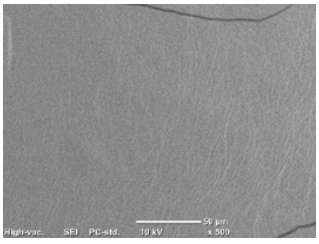	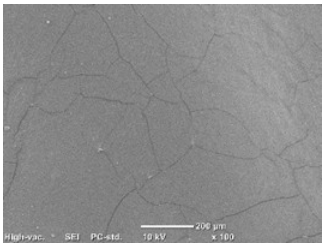
TPS-CH-M5	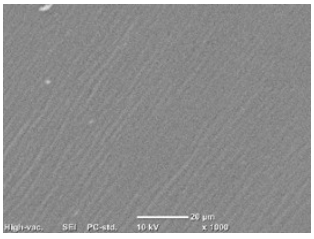	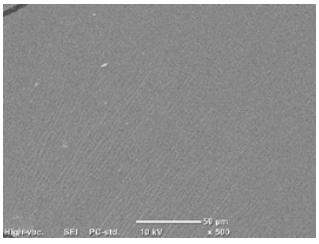	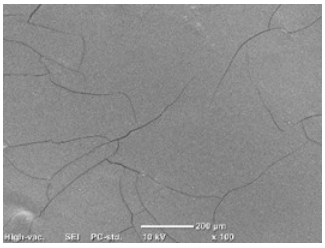

3.5. Mechanical Properties

Mechanical testing revealed that maltodextrin concentration directly influenced the tensile strength and elongation of the films. Sample TPS-CH-M3 exhibited the highest tensile strength (12.5 ± 1.2 MPa) and a moderate elongation at break (18 ± 2%), indicating an optimal balance between stiffness and flexibility. This behaviour is attributed to the formation of semicrystalline domains, as evidenced by the XRD analyses, which reinforce the matrix without compromising its elasticity [36]. In contrast, sample TPS-CH-M5 showed reduced tensile strength (8.3 ± 0.9 MPa) and increased brittleness, likely due to the formation of heterogeneous microdomains and internal stresses during drying, as observed in the SEM images (Figure 4). These results align with previous reports indicating that an excess of polysaccharides can generate discontinuities within the matrix, thereby diminishing its mechanical integrity [43]. The film without maltodextrin (TPS-CH-M0) exhibited low tensile strength (6.1 ± 0.7 MPa) and high stiffness, reaffirming the critical role of maltodextrin as a modifier of mechanical properties.

 doi:10.20944/preprints202605.0565.v1

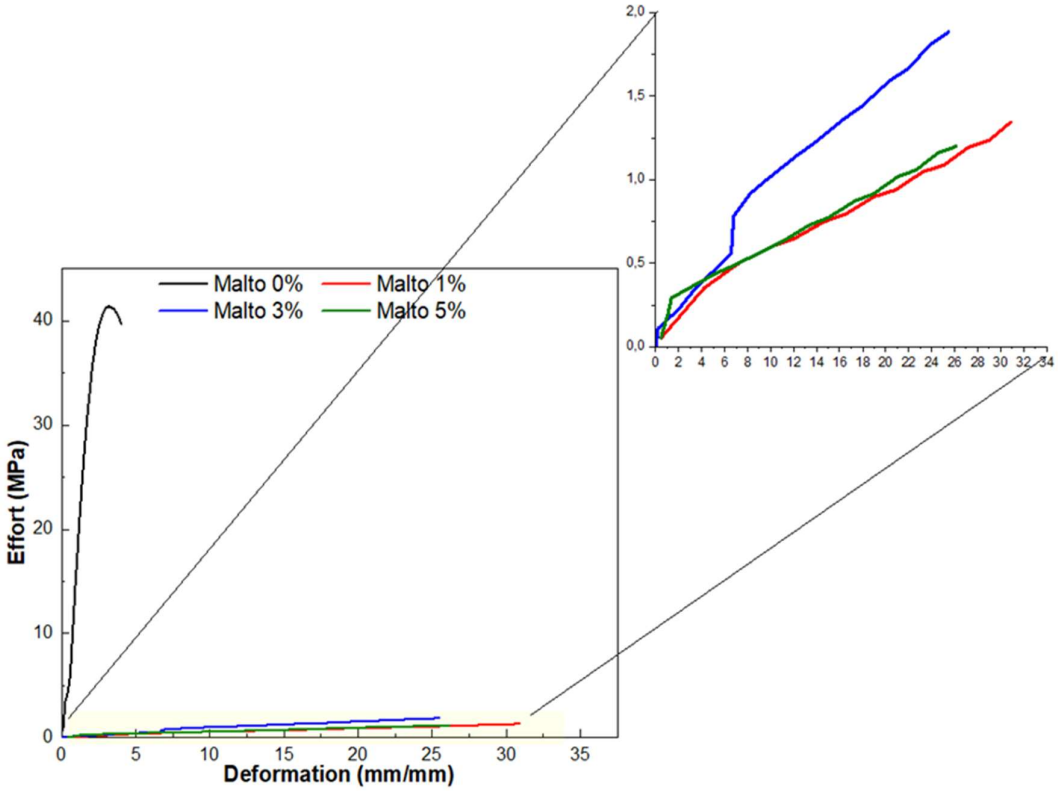

Figure 4. Stress–strain curves of TPS-CH-M films with different maltodextrin concentrations (0%, 1%, 3%, and 5%).

3.6. Fourier Transform Infrared Spectroscopy (FTIR)

Figure 6 presents the FTIR spectra of the formulations based on starch, chitosan, and maltodextrin. A broad band between 3600 and 3000 cm^{-1} is primarily attributed to the O–H stretching vibrations of the multiple hydroxyl groups present in both the plasticizer (glycerol) and the polymer chains of the biopolymers. The broadening of this band suggests the formation of intramolecular hydrogen bonds among these components, originating from attractive dipole–dipole interactions [42,44]. In this same region, overlapping signals corresponding to N–H stretching of amino groups (–NH) characteristic of chitosan are also observed. Additionally, bands associated with the asymmetric and symmetric stretching of C–H bonds in methyl and methylene groups appear at 2929 and 2885 cm^{-1}, respectively [18]. The band around ~1650 cm^{-1} is attributed to the bending vibration of O–H from adsorbed water and to the C=O stretching (amide I) of chitosan, originating from its residual acetyl groups [45]. A key spectral region lies between ~1300 and 949 cm^{-1}, corresponding to C–O vibrations in ether-related structures. The variations observed in this interval are associated with the formation of hydrogen bonds among the components [46].

In the fingerprint region, bands at 838 and 514 cm^{-1} are identified, corresponding to characteristic vibrations of aromatic rings and out-of-plane deformations of phenyl rings, respectively. The band at approximately 991 cm^{-1} is associated with the C–O stretching vibration in the anhydroglucose ring (C–O–C) and with intramolecular hydrogen bonding of hydroxyl groups at C-6, which is characteristic of the amorphous fraction of starch. Meanwhile, bands at 1083 and 1158 cm^{-1} are related to C–O and C–OH bending vibrations and are commonly used to estimate the proportion of crystalline phase in the material [47]. The presence of these bands in all formulations confirms that the main functional groups of each biopolymer remain intact and that no new signals indicative of intramolecular chemical reactions are detected. This suggests that the predominant interactions within the system are physical, mainly involving hydrogen bonds and dipole–dipole forces. Such

 doi:10.20944/preprints202605.0565.v1

interactions improve compatibility among starch, chitosan, and maltodextrin while preserving the structural integrity of the matrix—an essential characteristic for applications in controlled-release systems for active ingredients.

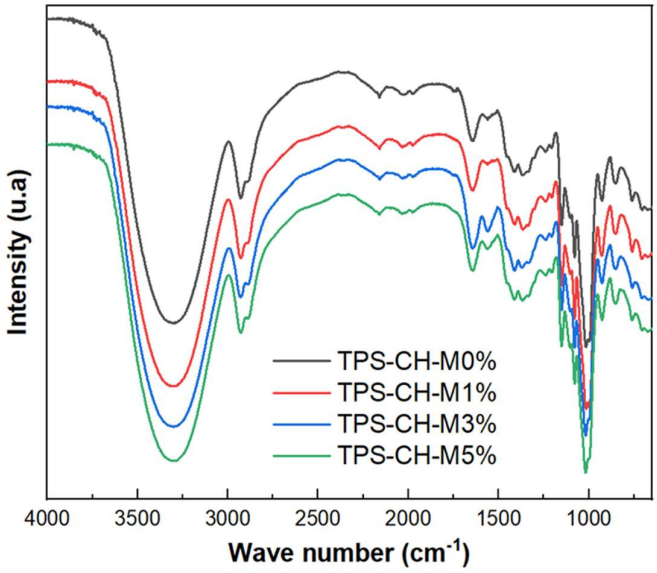

Figure 5. FTIR spectra of TPS-CH-M0, TPS-CH-M1, TPS-CH-M3, and TPS-CH-M5 in the range 4000–500 cm^{-1}.

3.7. Colorimetric Analysis

Table 5 summarizes the mean values of the color parameters ΔL, Δa, and Δb for films produced with different maltodextrin concentrations. The parameter ΔL is associated with material lightness, ranging from 0 (black) to 100 (white), and enables the identification of changes in sample brightness or darkening [48]. Across all formulations, ΔL values remained high, between 96.93 and 93.45, indicating that the films retained a clear appearance, although a slight darkening was observed as maltodextrin content increased.

The parameter Δa represents the tendency toward red hues when positive and toward green hues when negative [49]. All formulations exhibited negative Δa values, indicating a predominance of greenish tones [48]. Films containing maltodextrin showed more negative Δa values (less than −2), suggesting an enhanced greenish component compared with the control formulation.The Δb parameter, which reflects the intensity of yellow (positive values) or blue (negative values) tones, was positive in all samples, indicating a predominance of yellow coloration[48,50]. The Δb values increased with the addition of maltodextrin, indicating an intensification of yellow tonality. This effect may be attributed to the hydroxyl groups in the polysaccharide structure, which can promote oxidation or caramelisation reactions during the drying process [50]. Finally, the ΔE index, which quantifies the total colour difference with respect to the white reference, increased progressively with maltodextrin concentration, reaching values greater than 10 for TPS-CH-M5. These colour changes, along with the associated increase in opacity, suggest that this formulation may offer an effective barrier against UV radiation [49]. These results align with previous studies indicating that biopolymers such as maltodextrin can produce perceptible modifications in the colour profile of polymeric matrices [50].

 doi:10.20944/preprints202605.0565.v1

Table 6. Color and transparency parameters of TPS-CH-M films with different maltodextrin concentrations.

Color	L	a	b	ΔL	Δa	Δb	ΔE
Blanco	96,93	-0,04	1,78	-0,17	-0,08	0,11	0,22
TPS-CH-M0	93,89	-0,50	5,50	-3,22	-0,54	3,83	5,03
	94,22	-0,51	5,56	-2,88	-0,55	3,88	4,87
	94,63	-0,54	6,11	-2,47	-0,58	4,44	5,12
TPS-CH-M1	93,06	-1,32	9,50	-4,05	-1,35	7,83	8,92
	92,42	-1,50	10,26	-4,68	-1,54	8,59	9,91
	93,11	-1,39	8,66	-3,99	-1,43	6,99	8,18
TPS-CH-M3	93,66	-1,74	8,20	-3,45	-1,78	6,53	7,59
	93,45	-2,01	9,16	-3,65	-2,05	7,49	8,58
	93,40	-2,13	9,50	-3,70	-2,17	7,83	8,93
TPS-CH-M5	93,73	-2,12	10,43	-3,37	-2,16	8,76	9,63
	93,16	-2,27	10,96	-3,94	-2,31	9,29	10,35
	93,45	-2,42	11,11	-3,65	-2,45	9,44	10,41

4. Conclusions

The present study demonstrates that the incorporation of maltodextrin has a significant influence on the structural, thermal, surface, and mechanical properties of thermoplastic starch–chitosan polymer matrices, using TPS-CH-M0 (0% maltodextrin) as the reference formulation. X-ray diffraction analysis revealed that TPS-CH-M0 exhibited a predominantly amorphous character. In contrast, TPS-CH-M3 suggesting a more balanced and stable structural arrangement.

Simultaneous DSC and TGA analyses confirmed that maltodextrin incorporation increases the glass transition temperature in the reference TPS-CH-M0 and TPS-CH-M5, reflecting higher molecular rigidity and restricted polymer-chain mobility. Wettability measurements revealed that maltodextrin addition enhanced the hydrophilicity of the films compared with TPS-CH-M0. The contact angle decreased progressively in TPS-CH-M0 to TPS-CH-M3 and TPS-CH-M5. This increased wettability favours interaction with aqueous media, which is essential for controlled release of active ingredients. SEM micrographs showed that, while TPS-CH-M0 exhibited a relatively homogeneous surface, maltodextrin incorporation increased roughness and promoted the formation of microdomains. In TPS-CH-M3, these features remained controlled and compatible with the matrix; however, in TPS-CH-M5 they resulted in wrinkled and fragmented surfaces, reducing structural integrity. Mechanical testing confirmed that the film TPS-CH-M3 maintaining moderate tensile strength vs elongation at break. FTIR spectra demonstrated that maltodextrin incorporation did not generate new chemical signals relative to the TPS-CH-M0 reference. The main functional groups remained intact, and the interactions among components were primarily physical. Colorimetric analysis showed that the Maltodextrin incorporation slightly reduced this value and increased the yellow component without compromising material functionality. These colour changes, together with increased opacity, support the potential use of these films in packaging or coating applications for light-sensitive foods. Overall, a maltodextrin concentration of 3% was identified as the most suitable condition to optimize structural order, thermal stability, hydrophilicity, and mechanical performance of thermoplastic starch–chitosan matrices, while preserving their functional and spectroscopic integrity. These combined properties position TPS-CH-M3 as a promising candidate for use as a controlled-release vehicle for active ingredients in biomedical and food-packaging applications.

 doi:10.20944/preprints202605.0565.v1

Author Contributions: Author Contributions: Conceptualization, C.C. and A.F.-G.; methodology, M.C.R., C.A.-G., C.C., A.F.-G., M.E.T.-M., A.R.V.-A. and J.A.B.-B.; software, C.C., A.F.-G., M.E.T.-M., A.R.V.-A. and J.A.B.-B.; validation, C.C., A.F.-G., M.E.T.-M., A.R.V.-A. and J.A.B.-B.; formal analysis, M.C.R., C.A.-G., C.C., A.F.-G., M.E.T.-M., A.R.V.-A. and J.A.B.-B.; investigation, M.C.R., C.A.-G., C.C., A.F.-G., M.E.T.-M., A.R.V.-A. and J.A.B.-B.; resources, M.C.R., C.A.G., C.C., A.F.-G., M.E.T.-M., A.R.V.-A. and J.A.B.-B.; data curation, C.C. and A.F.-G.; writing—original draft preparation, M.C.R., C.A.-G., C.C., A.F.-G., M.E.T.-M., A.R.V.-A. and J.A.B.-B.; writing—review and editing, C.C. and A.F.-G.; visualization, M.C.R., C.A.-G., C.C., A.F.-G., M.E.T.-M., A.R.V.-A. and J.A.B.-B.; supervision, C.C. and A.F.-G.; project administration, C.C. and A.F.-G.; funding acquisition, C.C. and A.F.-G. All authors have read and agreed to the published version of the manuscript.

Funding: This research was funded by Vice-Rector for Research of Unidad Central del Valle del Cauca under project No.PI-1300-50.2-2026-26.

Institutional Review Board Statement: Not applicable.

Informed Consent Statement: Not applicable.

Data Availability Statement: The original contributions presented in this study are included in the article. Further inquiries can be directed to the corresponding author.

Acknowledgments: The authors extend thanks to IQ. Alfonso Mercado Silva, M. C. Gilberto Francisco Hurtado López, IQ. Beatriz E. Reyes Vielma, IQ. Ma. Guadalupe Mendez Padilla, Dr. Israel Sifuentes Nieves and LCQ Marlene Rodríguez Rodríguez for the technical support.

Conflicts of Interest: The authors declare no conflicts of interest.

References

1. Özakar, R.S.; Özakar, E. Current overview of oral thin films. *Turkish J. Pharm. Sci.* **2021**, *18*, 111–121. https://doi.org/10.4274/tjps.galenos.2020.76390
2. Ruggeri, M.; Bianchi, E.; Rossi, S.; Boselli, C.; Cornaglia, A.I.; Malavasi, L.; Carzino, R.; Suarato, G.; Sánchez-Espejo, R.M.; Athanassiou, A.; Viseras, C.; Ferrari, F.; Sandri, G. Maltodextrin-amino acids electrospun scaffolds cross-linked with Maillard-type reaction for skin tissue engineering. *Mater. Sci. Eng. C* **2021**, *133*, 112593. https://doi.org/10.1016/j.msec.2021.112593
3. Gupta, A.K.; Choudhari, A.; Kumar, A.; Kumar, A.; Gupta, A.; Faisal, S.; Kumar, A. Composites for drug-eluting devices: Emerging biomedical applications. In *Applications of Biotribology in Biomedical Systems*; Kumar, A., Kumar, A., Kumar, A., Eds.; Springer Nature: Cham, Switzerland, 2024; pp. 251–311. https://doi.org/10.1007/978-3-031-58327-8_10
4. González, Z.; Ferrandez-Montero, A.; Domínguez-Robles, J. Recent advances in polymers as matrices for drug delivery applications. *Pharmaceuticals* **2023**, *16*, 1674. https://doi.org/10.3390/ph16121674
5. Sung, Y.K.; Kim, S.W. Recent advances in polymeric drug delivery systems. *Biomater. Res.* **2020**, *24*, 12. https://doi.org/10.1186/s40824-020-00190-7
6. Borandeh, S.; van Bochove, B.; Teotia, A.; Seppälä, J. Polymeric drug delivery systems by additive manufacturing. *Adv. Drug Deliv. Rev.* **2021**, *173*, 349–373. https://doi.org/10.1016/j.addr.2021.03.022
7. Nguyen, H.X.; Banga, A.K. Fabrication, characterization and application of sugar microneedles for transdermal drug delivery. *Ther. Deliv.* **2017**, *8*, 249–264. https://doi.org/10.4155/tde-2016-0096
8. Buwalda, S.J.; Boere, K.W.M.; Dijkstra, P.J.; Feijen, J.; Vermonden, T.; Hennink, W.E. Hydrogels in a historical perspective: From simple networks to smart materials. *Biomacromolecules* **2018**, *19*, 316–330. https://doi.org/10.1021/acs.biomac.8b01234
9. Nyamba, I.; Sombie, C.B.; Yabre, M.; Zime-Diawara, H.; Yameogo, J.; Ouedraogo, S.; Lechanteur, A.; Semde, R.; Evrard, B. Pharmaceutical approaches for enhancing solubility and oral bioavailability of poorly soluble drugs. *Eur. J. Pharm. Biopharm.* **2024**, Article 114513. https://doi.org/10.1016/j.ejpb.2024.114513
10. Talat Mehrabad, J.; Arjomandi Rad, F.; Molaei, M. Molecular simulation of gabapentin intercalation in the interlayer space of Zn^{2+} Al-LDH: Molecular dynamics of drug delivery. *Chem. Rev. Lett.* **2025**, *8*, 11–19. https://doi.org/10.22034/crl.2024.469191.1389

 doi:10.20944/preprints202605.0565.v1

11. Yousefnezhad, M.; Babazadeh, M.; Davaran, S.; Akbarzadeh, A.; Pazoki-Toroudi, H. Preparation and in vitro evaluation of PCL–PEG–PCL nanoparticles for doxorubicin–ezetimibe co-delivery against PC3 prostate cancer cell line. *Chem. Rev. Lett.* **2024**, *7*, 159–172. https://doi.org/10.22034/crl.2024.436907.1285
12. Biswal, D.; Anupriya, B.; Uvanesh, K.; Anis, A.; Banerjee, I.; Pal, K. Effect of mechanical and electrical behavior of gelatin hydrogels on drug release and cell proliferation. *J. Mech. Behav. Biomed. Mater.* **2016**, *53*, 174–186. https://doi.org/10.1016/j.jmbbm.2015.08.017
13. García-Astrain, C.; Guaresti, O.; González, K.; Santamaria-Echart, A.; Eceiza, A.; Corcuera, M.A.; Gabilondo, N. Click gelatin hydrogels: Characterization and drug release behaviour. *Mater. Lett.* **2016**, *182*, 134–137. https://doi.org/10.1016/j.matlet.2016.06.115
14. Soe, M.T.; Pongjanyakul, T.; Limpongsa, E.; Jaipakdee, N. Modified glutinous rice starch–chitosan composite films for buccal delivery of hydrophilic drug. *Carbohydr. Polym.* **2020**, *245*, 116556. https://doi.org/10.1016/j.carbpol.2020.116556
15. Garavand, Y.; Taheri-Garavand, A.; Garavand, F.; Shahbazi, F.; Khodaei, D.; Cacciotti, I. Starch-polyvinyl alcohol-based films reinforced with chitosan nanoparticles: Physical, mechanical, structural, thermal and antimicrobial properties. *Appl. Sci.* **2022**, *12*, 1111. https://doi.org/10.3390/app12031111
16. Salgado, R.M.; Cruz-Castañeda, O.; Elizondo-Vázquez, F.; Pat, L.; De la Garza, A.; Cano-Colín, S.; Baena-Ocampo, L.; Krötzsch, E. Maltodextrin/ascorbic acid stimulates wound closure by increasing collagen turnover and TGF-β1 expression in vitro and changing the stage of inflammation from chronic to acute in vivo. *J. Tissue Viability* **2017**, *26*, 131–137. https://doi.org/10.1016/j.jtv.2017.01.004
17. Zanoelo, M.; Barbosa-Dekker, A.M.; Dekker, R.F.H.; Pereira, E.A.; Cunha, M.A.A. Microencapsulation of roasted mate tea extractives with lasiodiplodan (1→6)-β-D-glucan and maltodextrin as combined coating materials: A strategic tool to stabilize and protect bioactive components. *Int. J. Biol. Macromol.* **2024**, *267*, 133615. https://doi.org/10.1016/j.ijbiomac.2024.133615
18. Caicedo, C.; Ramírez-Giraldo, N.; Portilla, L.; Saldaña, L.; González-Pérez, G.; Fonseca-García, A. Physicochemical properties and in vitro dissolution of orally disintegrating films based on polysaccharides: The case of acetaminophen. *Appl. Sci.* **2025**, *15*, 4084. https://doi.org/10.3390/app15084084
19. Meena, S.; Prasad, W.; Khamrui, K.; Mandal, S.; Bhat, S. Preparation of spray-dried curcumin microcapsules using a blend of whey protein with maltodextrin and gum arabica and its in vitro digestibility evaluation. *Food Biosci.* **2021**, *41*, 100990. https://doi.org/10.1016/j.fbio.2021.100990
20. Anwar, D.M.; Khattab, S.N.; Helmy, M.W.; Kamal, M.K.; Bekhit, A.A.; Elkhodairy, K.A.; Elzoghby, A.O. Lactobionic/folate dual-targeted amphiphilic maltodextrin-based micelles for targeted codelivery of sulfasalazine and resveratrol to hepatocellular carcinoma. *Bioconjugate Chem.* **2018**, *29*, 3026–3042. https://doi.org/10.1021/acs.bioconjchem.8b00428
21. Yu, J.Y.; Roh, S.H.; Park, H.J. Characterization of ferulic acid encapsulation complexes with maltodextrin and hydroxypropyl methylcellulose. *Food Hydrocoll.* **2021**, *111*, 106390. https://doi.org/10.1016/j.foodhyd.2020.106390
22. Cilurzo, F.; Cupone, I.E.; Minghetti, P.; Selmin, F.; Montanari, L. Fast dissolving films made of maltodextrins. *Eur. J. Pharm. Biopharm.* **2008**, *70*, 895–900. https://doi.org/10.1016/j.ejpb.2008.06.032
23. Zhu, S.; Qiu, Z.; Qiao, X.; Waterhouse, G.I.; Zhu, W.; Zhao, W.; He, Q.; Zheng, Z. Creating burdock polysaccharide-oleanolic acid-ursolic acid nanoparticles to deliver enhanced anti-inflammatory effects: Fabrication, structural characterization and property evaluation. *Food Sci. Hum. Wellness* **2022**, *12*, 454–466. https://doi.org/10.1016/j.fshw.2022.07.047
24. Combo, A.M.M.; Aguedo, M.; Quiévy, N.; Danthine, S.; Goffin, D.; Jacquet, N.; Blecker, C.; Devaux, J.; Paquot, M. Characterization of sugar beet pectic-derived oligosaccharides obtained by enzymatic hydrolysis. *Int. J. Biol. Macromol.* **2012**, *52*, 148–156. https://doi.org/10.1016/j.ijbiomac.2012.09.006
25. Desoky, M.M.; Hoti, G.; Tsaturyan, A.; Cecone, C.; Caldera, F.; Trotta, F. Green synthesis of scalable non-soluble hydrogels: Rapid transesterification of maltodextrin with dimethyl carbonate using DABCO/DMSO. *Green Chem.* **2025**, *27*, 8649–8659. https://doi.org/10.1039/d5gc02156a
26. Dee, G.T.; Sauer, B.B. The cohesive energy density of polymers and its relationship to surface tension, bulk thermodynamic properties, and chain structure. *J. Appl. Polym. Sci.* **2016**, *134*. https://doi.org/10.1002/app.44431

 doi:10.20944/preprints202605.0565.v1

27. Wongphan, P.; Harnkarnsujarit, N. Characterization of starch, agar and maltodextrin blends for controlled dissolution of edible films. *Int. J. Biol. Macromol.* **2020**, *156*, 80–93. https://doi.org/10.1016/j.ijbiomac.2020.04.056
28. Zhou, X.; Wu, S.; Liu, P.; Wang, L.; Xie, F. Hybrid bioink of methacrylated starch with minimal methacrylated chitosan enables high-precision 3D printing for complex tissue scaffolds. *Carbohydr. Polym.* **2025**, *367*, 124023. https://doi.org/10.1016/j.carbpol.2025.124023
29. Hernández, M.S.; Ludueña, L.N.; Flores, S.K. Combined effect of oregano essential oil and glycerol on physicochemical properties of antimicrobial films based on chitosan and acetylated cassava starch. *Food Hydrocoll.* **2024**, *156*, 110259. https://doi.org/10.1016/j.foodhyd.2024.110259
30. Cyras, V.P.; D'Amico, D.A.; Manfredi, L.B. Crystallization behavior of polymer nanocomposites. In *Crystallization in Multiphase Polymer Systems*; Thomas, S., Arif, M., Gowd, E.B., Eds.; Elsevier: Amsterdam, Netherlands, **2018**; pp. 201–228. https://doi.org/10.1016/B978-0-12-809453-6.00008-1
31. Samaniego-Aguilar, K.; Sánchez-Safont, E.; Pisa-Ripoll, I.; Torres-Giner, S.; Flores, Y.; Lagaron, J.M.; Cabedo, L.; Gamez-Perez, J. Performance enhancement of biopolyester blends by reactive compatibilization with maleic anhydride-grafted poly(butylene succinate-co-adipate). *Polymers* **2024**, *16*, 2325. https://doi.org/10.3390/polym16162325
32. Huang, Y.; Yu, H.; Xiao, C. pH-sensitive cationic guar gum/poly(acrylic acid) polyelectrolyte complex hydrogels for drug delivery. *Polym. Degrad. Stab.* **2012**, *97*, 1197–1205. https://doi.org/10.1016/j.polymdegradstab.2012.05.019
33. Abubakar, A.S.; Ahmad, B.; Ahmad, N.; Liu, L.; Liu, B.; Qu, Y.; Chen, J.; Chen, P.; Zhao, H.; Chen, J.; Chen, K.; Gao, G.; Zhu, A. Physicochemical evaluation, structural characterization, in vitro and in vivo bioactivities of water-soluble polysaccharides from *Apocynum* tea. *Food Chem.* **2024**, *460*, 140453. https://doi.org/10.1016/j.foodchem.2024.140453
34. Rodríguez, I.; Gautam, R.; Tinoco, A.D. Use of X-ray diffraction techniques for the development, formulation and polymorphic characterization of biomimetic drugs. *Biomimetics* **2021**, *6*, 1. https://doi.org/10.3390/biomimetics6010001
35. Tafa, K.D.; Satheesh, N.; Abera, W. Mechanical properties of tef starch-based edible films: Development and process optimization. *Heliyon* **2023**, *9*, e13160. https://doi.org/10.1016/j.heliyon.2023.e13160
36. Callister, W.D.; Rethwisch, D.G. *Materials Science and Engineering: An Introduction*, 10th ed.; Wiley: Hoboken, NJ, USA, 2020.
37. dos Santos, W.N.; De Sousa, J.A.; Gregorio, R. Thermal conductivity behaviour of polymers around glass transition and crystalline melting temperatures. *Polym. Test.* **2013**, *32*, 987–994. https://doi.org/10.1016/j.polymertesting.2013.05.007
38. Sperling, L.H. *Introduction to Physical Polymer Science*, 4th ed.; Wiley: Hoboken, NJ, USA, 2016.
39. Tan, S.X.; Ong, H.C.; Andri, A.; Lim, S.; Kusumo, F.; Pang, Y.L.; Ngoh, G.C. Characterization and parametric study on mechanical properties enhancement in biodegradable chitosan-reinforced starch-based bioplastic film. *Polymers* **2022**, *14*, 278. https://doi.org/10.3390/polym14020278
40. Panraksa, P.; Qi, S.; Udomsom, S.; Tipduangta, P.; Rachtanapun, P.; Jantanasakulwong, K.; Jantrawut, P. Characterization of hydrophilic polymers as a syringe extrusion 3D printing material for orodispersible film. *Polymers* **2021**, *13*, 3454. https://doi.org/10.3390/polym13203454
41. Sothornvit, R.; Krochta, J.M. Plasticizer effect on mechanical properties of β-lactoglobulin films. *J. Food Eng.* **2000**, *50*, 149–155. https://doi.org/10.1016/S0260-8774(00)00194-0
42. Liu, H.; Adhikari, R.; Guo, Q.; Adhikari, B. Preparation and characterization of glycerol plasticized (high-amylose) starch–chitosan films. *J. Food Eng.* **2013**, *116*, 588–597. https://doi.org/10.1016/j.jfoodeng.2012.12.037
43. Zhang, R.; Wang, W.; Zhang, H.; Dai, Y.; Dong, H.; Hou, H. Effects of hydrophobic agents on the physicochemical properties of edible agar/maltodextrin films. *Food Hydrocoll.* **2018**, *88*, 283–290. https://doi.org/10.1016/j.foodhyd.2018.10.008
44. Bajer, D.; Janczak, K.; Bajer, K. Novel starch/chitosan/aloe vera composites as promising biopackaging materials. *J. Polym. Environ.* **2020**, *28*, 1021–1039. https://doi.org/10.1007/s10924-020-01661-7

 doi:10.20944/preprints202605.0565.v1

45. Wan, Y.; Wu, H.; Yu, A.; Wen, D. Biodegradable polylactide/chitosan blend membranes. *Biomacromolecules* **2006**, *7*, 1362–1372. https://doi.org/10.1021/bm0600825
46. Sritham, E.; Gunasekaran, S. FTIR spectroscopic evaluation of sucrose–maltodextrin–sodium citrate bioglass. *Food Hydrocoll.* **2017**, *70*, 371–382. https://doi.org/10.1016/j.foodhyd.2017.04.023
47. Guo, J.; Liu, L.; Lian, X.; Li, L.; Wu, H. The properties of different cultivars of Jinhai sweet potato starches in China. *Int. J. Biol. Macromol.* **2014**, *67*, 1–6. https://doi.org/10.1016/j.ijbiomac.2014.03.002
48. Woszczak, L.; Khachatryan, K.; Krystyjan, M.; Witczak, T.; Witczak, M.; Gałkowska, D.; Makarewicz, M.; Khachatryan, G. Physicochemical and functional properties and storage stability of chitosan–starch films containing nano/microstructures with turmeric and hibiscus extracts. *Int. J. Mol. Sci.* **2023**, *24*, 12218. https://doi.org/10.3390/ijms241512218
49. Okutan, G.; Koç, G.; Cansu, Ü.; Boran, G. Edible films based on plant and animal origin proteins: Comparison of mechanical and physicochemical characteristics. *Food Sci. Nutr.* **2025**, *13*. https://doi.org/10.1002/fsn3.4712
50. Ma, S.; Zheng, Y.; Zhou, R.; Ma, M. Characterization of chitosan films incorporated with konjac glucomannan, cassava starch, maltodextrin and gelatin. *Coatings* **2021**, *11*, 84. https://doi.org/10.3390/coatings11010084